Research Article

Najeeb Alam Khan*, Farah Naz, and Faqiha Sultan

Entropy generation analysis and effects of slip conditions on micropolar fluid flow due to a rotating disk

https://doi.org/10.1515/eng-2017-0025
Received Feb 02, 2017; accepted May 30, 2017

Abstract: This article deals with the investigation of three-dimensional axisymmetric steady flow of micropolar fluid over a rotating disk in a slip-flow regime. Further, the generation of entropy due to heat transfer and fluid friction is identified. It is noticed that the entropy generation can be decreased and controlled in the presence of slip. The anisotropic slip has vital characteristics and it has a great influence on the flow field and heat transfer. The von Kármán similarity transformation is used to establish the equations governing the flow and heat transfer characteristics of the fluid. The impact of some important parameters on velocity profiles, angular velocity (microrotation) and energy distribution is discussed and illustrated through graphs and tables. The effects of physical parameters on the entropy generation and Bejan numbers are also presented graphically. In addition, the most favorable agreement is observed among the results of the present study and those of the earlier studies.

Keywords: Micropolar; anisotropic slip; entropy generation; rotating disk; axisymmetric

1 Introduction

In the last few years, the dynamical study of non-Newtonian fluids has got vital attention among various researchers. The flow produced from these type of fluids can be used to analyze a broader class of fluids that exist in the physical world. The distinctive property of non-Newtonian fluids is to have the variable viscosity. Non-Newtonian fluids are rheologically complex fluids represented by the non-linear relationships among shear stress and strain rate. The micropolar fluid model, also known as polar fluid, is one of the non-Newtonian models that have microstructure. Micropolar fluids come into the category of fluids that have nonsymmetrical stress tensor and consist of stiff and arbitrarily structured particles hanging in a viscous channel where the deformation of fluid particles is uncountable. In recent times, a lot of researchers have been giving their attention to the theory of micropolar fluids and this is because conventional Newtonian fluids does not have the ability to explain the properties of the fluid flows containing suspended particles. The main reason for the significant attention to the investigation of the flows of micropolar fluids was their usages and applications in different industrial processes, which include: solidification of liquid crystal, the extrusion of polymer fluids, animal blood, exotic lubricants, cooling of a metallic plate in a bath, and colloidal and suspension solutions. More complex fluids can be described by the extension of Newtonian fluids to the theory of micropolar fluid flow. Eringen [1] presented a model which consists of special types of fluids known as microfluids. These fluids are composed of randomly structured rigid particles suspended in a viscous medium and have essential microscopic characteristics. The theory of micropolar fluids received a lot of attention among the researchers [2–5]. The main reason for the advances in Eringen's microcontinuum mechanics was the introduction of new kinematic variables, for instance, the microinertia moment and gyration tensors, and also to include the ideas of stress moments, body moments, and microstress. Ariman, *et al.* [6] discussed the theory of micropolar fluids that consists of the effects arising from the intrinsic motion of fluid elements and their micropolar structure. Chamkha, *et al.* [7] applied the boundary layer theory to examine the three-dimensional flow of a micropolar fluid due to a continuous stretching surface by using similarity assumptions. Ashraf and Batool [8] proposed the nu-

***Corresponding Author: Najeeb Alam Khan:** Department of Mathematics, University of Karachi, Karachi 75270, Pakistan; Email: njbalam@yahoo.com
Farah Naz: Department of Mathematics, University of Karachi, Karachi 75270, Pakistan
Faqiha Sultan: Department of Sciences and Humanities, National University of Computer and Emerging Sciences, Karachi 75030, Pakistan

merical study based on the axisymmetric laminar flow of micropolar fluid due to a stretchable disk while taking the magnetic field effect on the flow. Borrelli, *et al.* [9] studied the three-dimensional stagnation point flow of a micropolar fluid subjected to the magnetic effects and proposed the numerical results of governing equations of the flow. Hussain, *et al.* [10] obtained the solution of the problem established by the flow of a micropolar fluid rotating about an accelerated disk.

The study of fluid flow due to a rotating disk has become increasingly popular in fluid dynamic research for the interest not only practical but also academic. The flow over a rotating disk is important because of its wide applications in many engineering, industrial, geothermal, geophysical, and technological fields. Kármán [11] investigated the fluid flow due to an infinite rotating disk that proved to be a revolutionary study in the field of fluid mechanics. He was the first to propose the similarity transformation for the rotating disk flow problems that is used to transform the governing partial differential equations into ordinary differential equations. The similarity analysis of the rotating disk flow by Kármán led to various investigations that have been carried out for the flow fields regarding disk flows. Turkyilmazoglu [12] investigated the solution of an electrically conducting fluid flow and extended the Kármán viscous pump problem by taking the flow over a radially stretchable rotating disk under the influence of a uniform vertical magnetic effect and examined the magnetic effects on the flow. The steady flow of an incompressible power law fluid due to rotating infinite disk was studied by Ming, *et al.* [13] and they provided the numerical results of the fluid flow with heat transfer effect. Rashidi, *et al.* [14] have developed a set of nonlinear partial differential equations that corresponded with the steady convective and magnetohydrodynamic (MHD) slip flow occurred due to the rotation of a disk in the existence of viscous dissipation and Ohmic heating.

The second law of thermodynamics is more reliable than the first because it reduces the sum of frictional and thermal entropy generation rates. However, in the past few years, the second law analysis have been known as the exergy analysis of available energy. It has several useful applications in engineering because it offers the quantitative information about irreversibilities and exergy losses in the system. Exergy analysis improves the performance of engineering process that involves heat transfer and inspects the irreversibility in terms of entropy generation caused by the motion of fluid and heat transfer and predicts the performance of engineering processes. The viscous dissipation and heat transfer are the causes of the production of entropy. Pioneering work on the entropy generation in fluid flow has been done by Bejan [15, 16]. He also discussed the generation of entropy for the flow of forced convection viscous fluid in a channel as a result of viscous friction and heat transfer in the fluid. Many investigators were motivated to execute the analysis, subjected to the second law of thermodynamics. Abdollahzadeh Jamalabadi [17] presented and discussed the problem of the entropy generation in steady boundary layer flow of a micropolar fluid over a stretching sheet. Additionally, the heat and mass transfer features have also been taken into account on the flow field.

On reviewing the literature, it is well identified that the velocity profiles can be significantly affected by the existence of a slip boundary condition. As far as our knowledge is concerned, no significant attention has been given to investigate the slip effect on the fluid flow. However, Joseph [18] gave an idea of slip condition and discussed its eminent characteristic for reducing the skin friction. Many studies [19–21] are established to examine the slip effect on the different fluid flows and it has been noticed that the slip condition is significant to increase flow pressure when the characteristic size of the flow system is low. In recent past, the superhydrophobic surfaces have gained much importance and have become the subject of intense research because of their potential to decrease skin-friction drag. The superhydrophobic surfaces depend on directions and have different slip-length values in spanwise and streamwise directions. The effects on flows over superhydrophobic surfaces have also gained some attention. Busse and Sandham [22] analyzed the turbulent channel flow and observed the influence of an anisotropic Navier slip-length boundary condition.

Motivated by the aforementioned work, the present research examines the comprehensive study of micropolar fluid flow over a rotating disk along with anisotropic slip and the dissipation effects. The present study also examines the entropy generation characteristics for a rotating disk flow. Such effects have not been considered yet on a micropolar fluid. This study explores these effects of emerging flow parameters on the velocity profiles, microrotation, and temperature distribution.

2 Micropolar Fluid Model

In the present study, micropolar fluid is the fluid of interest, which has microscopic characteristics such as microrotational and rotational inertia. The fundamental equations for the micropolar fluid are written as:

$$\tau_i^j = (-p + divV)\,\delta_i^j + (2\mu + k)\,e_i^j + k\varepsilon_{ijm}\,(\omega - N)\,, \quad (1)$$

$$M_i^j = (\alpha div V)\,\delta_i^j + \beta\omega_{i,j} + \gamma\omega_{i,j} \tag{2}$$

Where, τ_i^j is the stress tensor, M_i^j is the couple stress tensor, e_i^j are the components of the rate of strain, p is the pressure, μ and k are viscosity coefficients, $(\alpha,\ \beta,\ \gamma)$ are the material constants of micropolar fluids, V denotes the velocity vector, N and ω indicate the microrotation vector and vorticity vector components respectively, ε_{ijm} is the Levi-Civita symbol, δ_i^j is the Kronecker delta and the comma in i, j gives covariant differentiation.

The stress components of micropolar fluid in cylindrical coordinates system are given by

$$\tau_r^r = 2\left(\mu + \frac{k}{2}\right)\frac{\partial u}{\partial r} \tag{3}$$

$$\tau_r^\psi = \left(\mu + \frac{k}{2}\right) r\frac{\partial}{\partial r}\left(\frac{v}{r}\right) + \frac{k}{2}\left(\frac{\partial v}{\partial r} + \frac{v}{r} - \frac{1}{r}\frac{\partial u}{\partial \psi}\right) - kN_3 \tag{4}$$

$$\tau_r^z = \left(\mu + \frac{k}{2}\right)\left(\frac{\partial u}{\partial z} + \frac{\partial w}{\partial r}\right) + \frac{k}{2}\left(\frac{\partial w}{\partial r} - \frac{\partial u}{\partial z}\right) + kN_2 \tag{5}$$

$$\tau_\psi^r = \left(\mu + \frac{k}{2}\right) r\frac{\partial}{\partial r}\left(\frac{v}{r}\right) + \frac{k}{2}\left(\frac{1}{r}\frac{\partial u}{\partial \psi} - \frac{\partial v}{\partial r} - \frac{v}{r}\right) + kN_3 \tag{6}$$

$$\tau_\psi^\psi = \frac{2}{r}\left(\mu + \frac{k}{2}\right) u \tag{7}$$

$$\tau_\psi^z = \left(\mu + \frac{k}{2}\right)\frac{\partial v}{\partial z} + \frac{k}{2}\left(\frac{1}{r}\frac{\partial w}{\partial \psi} - \frac{\partial v}{\partial z}\right) - kN_1 \tag{8}$$

$$\tau_z^r = \left(\mu + \frac{k}{2}\right)\left(\frac{\partial u}{\partial z} + \frac{\partial w}{\partial r}\right) + \frac{k}{2}\left(\frac{\partial u}{\partial z} - \frac{\partial w}{\partial r}\right) - kN_2 \tag{9}$$

$$\tau_z^\psi = \left(\mu + \frac{k}{2}\right)\frac{\partial v}{\partial z} + \frac{k}{2}\left(\frac{\partial v}{\partial z} - \frac{1}{r}\frac{\partial w}{\partial \psi}\right) + kN_1 \tag{10}$$

$$\tau_z^z = 2\left(\mu + \frac{k}{2}\right)\frac{\partial w}{\partial z} \tag{11}$$

In above equations, (r, ψ, z) are the components of cylindrical coordinates, (u, v, w) are the components of velocity vector, and (N_1, N_2, N_3) are the components of microrotation vector.

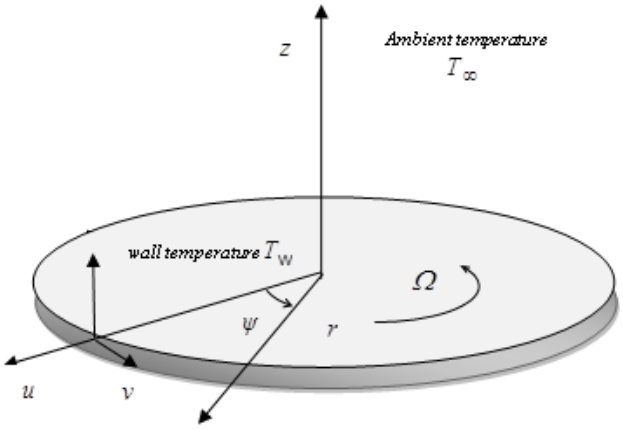

Figure 1: Geometrical configuration of the flow

2.1 Mathematical Description of the Problem

Assuming the steady, laminar, and axisymmetric flow of an incompressible non-Newtonian micropolar fluid over a rotating disk in slip-flow regime (Figure 1), which can be defined in three-dimensional frame of reference by using the cylindrical polar coordinates (r, ψ, z), where r is the radial distance from the axis, ψ is the polar angle, and z is the normal distance from the disk. Further, the constant temperature on the surface of the disk is assumed to be T_w and T_∞ is the temperature surrounding fluid. It is also assumed that the fluid flow is under slip boundary conditions, and the body couples and body force are likely to be neglected. All the flow quantities are independent of t and ψ as the flow is steady and axisymmetric. Thus, the components of velocity (u, v, w) and microrotation (N_1, N_2, N_3) along the radial, tangential, and axial directions are:

$$u = u(r,z),\ v = v(r,z),\ w = w(r,z),$$
$$N_1 = 0,\ N_2 = N_2(r,z),\ N_3 = 0.$$

Therefore, the equations governing the motion with the above assumptions are:

$$\frac{1}{r}\frac{\partial(r\rho u)}{\partial r} + \frac{\partial(\rho w)}{\partial z} = 0, \tag{12}$$

$$\rho\left(u\frac{\partial u}{\partial r} - \frac{v^2}{r} + w\frac{\partial u}{\partial z}\right) = -\frac{\partial p}{\partial r} + \frac{\partial \tau_r^r}{\partial r} + \frac{\partial \tau_z^r}{\partial z} + \frac{\tau_r^r - \tau_\psi^\psi}{r}, \tag{13}$$

$$\rho\left(u\frac{\partial v}{\partial r} + \frac{uv}{r} + w\frac{\partial v}{\partial z}\right) = \frac{\partial \tau_r^\psi}{\partial r} + \frac{\partial \tau_z^\psi}{\partial z} + \frac{2\tau_\psi^r}{r}, \tag{14}$$

$$\rho\left(u\frac{\partial w}{\partial r}+w\frac{\partial w}{\partial z}\right)=-\frac{\partial p}{\partial z}+\frac{\partial \tau_z^r}{\partial r}+\frac{\tau_r^z}{r}+\frac{\partial \tau_z^z}{\partial z}, \tag{15}$$

$$\begin{aligned}&\rho j\left(u\frac{\partial N_2}{\partial r}+w\frac{\partial N_2}{\partial z}\right) \\ &=\gamma\left(\frac{\partial^2 N_2}{\partial z^2}+\frac{1}{r}\frac{\partial N_2}{\partial r}-\frac{N_2}{r^2}+\frac{\partial^2 N_2}{\partial r^2}\right)+k\left(\frac{\partial u}{\partial z}-\frac{\partial w}{\partial r}\right) \\ &-2kN_2,\end{aligned} \tag{16}$$

$$\begin{aligned}&\rho C_p\left(u\frac{\partial T}{\partial r}+w\frac{\partial T}{\partial z}\right) \\ &=k_0\left(\frac{\partial^2 T}{\partial r^2}+\frac{1}{r}\frac{\partial T}{\partial r}+\frac{\partial^2 T}{\partial z^2}\right)+\varphi,\end{aligned} \tag{17}$$

Where,

$$\begin{aligned}\varphi=&2\left(\frac{\partial u}{\partial r}\right)\tau_r^r+2\left(\frac{1}{r}\frac{\partial v}{\partial \psi}+\frac{u}{r}\right)\tau_\psi^\psi+2\left(\frac{\partial w}{\partial z}\right)\tau_z^z \\ &+2\left(\left(\frac{1}{r}\frac{\partial u}{\partial \psi}+r\frac{\partial}{\partial r}\left(\frac{v}{r}\right)\right)\tau_r^\psi+\frac{\partial w}{\partial r}\tau_r^z+\frac{1}{r}\frac{\partial w}{\partial \psi}\tau_\psi^z\right)\end{aligned} \tag{18}$$

The subjected boundary conditions are

$$\begin{aligned}&u=k_1\tau_r^z,\ v=r\Omega+k_2\tau_\psi^z,\ w=0,\ T=T_w \text{ at } z=0, \\ &u\to 0,\ v\to 0,\ w\to 0,\ T\to T_\infty,\ p\to 0 \text{ as } z\to\infty\end{aligned} \tag{19}$$

Where, C_p is the specific heat at constant pressure, k_0 is the thermal conductivity, k_1 and k_2 are the slip coefficients in the radial and tangential directions, and φ is the dissipation function respectively.

2.2 Similarity Transformation

The flow is examined by the ordinary differential equations (ODEs) found by means of an appropriate non-dimensional transformation variable given by Kármán [11], adapted to reduce partial differential equations governing the axisymmetric momentum associated with the rotating disk flow into ODEs. The similarity variable is defined as:

$$\begin{aligned}&u=r\Omega F(\Lambda),\ v=r\Omega G(\Lambda), \\ &w=\sqrt{\nu\Omega}H(\Lambda),\ p=\rho\nu\Omega P(\Lambda),\ N_2=\left(\frac{r\Omega^{\frac{3}{2}}}{\sqrt{\nu}}\right)M(\Lambda) \\ &T=T_\infty+(T_w-T_\infty)\theta(\Lambda),\quad \Lambda=\sqrt{\frac{\Omega}{\nu}}z \text{ and } Re=\frac{\Omega r^2}{\nu}\end{aligned} \tag{20}$$

Where, the dimensionless functions F, G, and H are the dimensionless components of velocity along the radial, tangential, and axial directions, M is the dimensionless microrotation, $\nu=\frac{\mu}{\rho}$ is the kinematic viscosity, Λ is the dimensionless distance from the surface of the disk, Re is the Reynolds number, and p is the dimensionless hydraulic pressure above the disk. On applying the above transformation on Eqs. (12)-(18), the equations of continuity and momentum become:

$$2F(\Lambda)+H'(\Lambda)=0, \tag{21}$$

$$\begin{aligned}&(1+C_1)F''(\Lambda)-(F(\Lambda))^2+(G(\Lambda))^2 \\ &-H(\Lambda)F'(\Lambda)-C_1M'(\Lambda)=0,\end{aligned} \tag{22}$$

$$\begin{aligned}&(1+C_1)G''(\Lambda)-\frac{2C_1}{Re}G'(\Lambda)-2F(\Lambda)G(\Lambda) \\ &-H(\Lambda)G'(\Lambda)=0,\end{aligned} \tag{23}$$

$$P'(\Lambda)+(2+C_1)F'(\Lambda)-2H(\Lambda)F(\Lambda)=0, \tag{24}$$

$$\begin{aligned}&C_2M''(\Lambda)-F(\Lambda)M(\Lambda)+C_3F'(\Lambda) \\ &-H(\Lambda)M'(\Lambda)-2C_3M(\Lambda)=0,\end{aligned} \tag{25}$$

$$\begin{aligned}&\theta''(\Lambda)-\mathrm{Pr}\,H(\Lambda)\theta'(\Lambda) \\ &+Br\left(\begin{array}{l}\frac{1}{Re}\left(4\left(H'(\Lambda)\right)^2+2C_1\left(H'(\Lambda)\right)^2\right. \\ \left.+8(F(\Lambda))^2+4C_1(F(\Lambda))^2\right) \\ +2\left(\left(G'(\Lambda)\right)^2+\left(F'(\Lambda)\right)^2+C_1M(\Lambda)F'(\Lambda)\right)\end{array}\right)=0,\end{aligned} \tag{26}$$

subject to the boundary conditions:

$$\begin{aligned}&F(0)=\zeta\left(F'(0)+C_1M(0)\right),\ G(0)=1+\eta G'(0), \\ &H(0)=0,\ \theta(0)=1,\ P(0)=0\end{aligned} \tag{27}$$

and

$$F(\infty)=0,\ G(\infty)=0,\ \theta(\infty)=0 \tag{28}$$

Where, $C_1=\frac{k}{\mu}$ is vortex viscosity parameter, $C_2=\frac{\gamma}{\rho j\nu}$, $C_3=\frac{k}{\rho j\Omega}$ represent the spin gradient viscosity parameter and the microinertia density parameter, $\mathrm{Pr}=\frac{\mu C_p}{k_0}$ is the Prandtl number, and the Brinkman number is $Br=\frac{\mu\Omega^2r^2}{k_0\Delta T}$.

2.3 Physical Quantities

In Kármán flows, the coefficients of shear stress are the important physical quantities. The radial and circumferential shear stress coefficients of the micropolar fluid can be obtained by:

$$C_f=\left.\frac{\tau_r^z}{\mu\Omega}\right|_{z=0},\quad C_g=\left.\frac{\tau_\psi^z}{\mu\Omega}\right|_{z=0} \tag{29}$$

The skin friction coefficients C_f and C_g from Eq. (29) are obtained in dimensionless form as:

$$C_f = \sqrt{Re}\left(C_1 M(0) + F'(0)\right), \quad C_g = \sqrt{Re}G'(0) \tag{30}$$

The convective and conductive heat transfers in a fluid across the surface are interrelated with the help of Nusselt number, which is defined as:

$$N_u = \frac{q_w}{(T_w - T_\infty)} \tag{31}$$

Here, q_w is the heat flux at the surface of the rotating disk due to conduction.

$$q_w = -r\left(\frac{\partial T}{\partial z}\right)\Big|_{z=0} \tag{32}$$

Thus, the dimensionless form of the Nusselt number is obtained as:

$$N_u = -\sqrt{Re}\theta'(0) \tag{33}$$

3 Entropy Analysis

Entropy is a state function that shows the unidirectional nature of thermodynamic processes. It is the most significant thermodynamic characteristic that represents the chaos of a system and surroundings and so often, the entropy is known as the measure of chaos. The basic cause for the occurrence of entropy is the transfer of heat (energy) and when it happens, a number of movements appear such as molecular resistance, molecular vibration, inner molecular displacement, rotational moment, kinetic energy etc., which becomes the reason of disorderliness in a system and its surroundings. It emanates from the second law of thermodynamics, which is a second important idea in the field. The thermodynamic irreversibilities can be measured by considering the entropy generation analysis in the system and can be applied to any character of the energy conversion scheme. There are two sources of entropy generation, first is heat transfer along the direction of temperature gradients and second is the irreversibility due to fluid friction.

The volumetric rate of entropy generation for micropolar fluid flow in cylindrical coordinates is given as [23]:

$$\begin{aligned} S_G = \frac{1}{T_w}\Bigg(&2\left(\frac{\partial u}{\partial r}\right)\tau_r^r + 2\left(\frac{1}{r}\frac{\partial v}{\partial \psi} + \frac{u}{r}\right)\tau_\psi^\psi \\ &+ 2\left(\frac{\partial w}{\partial z}\right)\tau_z^z + 2\left(\left(\frac{1}{r}\frac{\partial u}{\partial \psi} + r\frac{\partial}{\partial r}\left(\frac{v}{r}\right)\right)\tau_r^\psi + \frac{\partial w}{\partial r}\tau_r^z \right. \\ &\left. + \frac{1}{r}\frac{\partial w}{\partial \psi}\tau_\psi^z\right)\Bigg) \\ &+ \frac{k_0}{(T_w)^2}\left(\left(\frac{\partial T}{\partial r}\right)^2 + \left(\frac{\partial T}{\partial z}\right)^2\right) \end{aligned} \tag{34}$$

The characteristic entropy generation rate S_{G0} can also be given as:

$$S_{G0} = \frac{k_0 \Omega (T_w - T_\infty)}{T_w \nu} \tag{35}$$

where k_0 represents thermal conductivity, ν is kinematic viscosity, and T_w is the channel's absolute reference temperature.

In dimensionless form, the entropy generation can be explained as the ratio of characteristic entropy transfer rate and the actual entropy generation rate, as reported by Bejan [23]. Thus, for each fluid with dimensionless variables, the entropy generation number is defined as:

$$\begin{aligned} N_G = \frac{S_G}{S_{G0}} = Br\Bigg(&\frac{1}{Re}\left(4C_1(F(\Lambda))^2 + 8(F(\Lambda))^2\right. \\ &\left. + 2C_1\left(H'(\Lambda)\right)^2 + 4\left(H'(\Lambda)\right)^2\right) \\ &+ 2\left(C_1 M(\Lambda) F'(\Lambda) + \left(F'(\Lambda)\right)^2 + \left(G'(\Lambda)\right)^2\right)\Bigg) \\ &+ (\sigma_1 - 2\sigma_2 + Q_0\sigma_2)\left(\theta'(\Lambda)\right)^2 \end{aligned} \tag{36}$$

where $\sigma_1 = \frac{T_w}{(T_w - T_\infty)}$, $\sigma_2 = \frac{T_\infty}{(T_w - T_\infty)}$ are the temperature ratios and $Q_0 = \frac{T_\infty}{T_w}$.

The Bejan number, also known as an alternative irreversibility distribution parameter, provides information concerning with irreversibility mechanism. It is the ratio of total entropy generation and entropy generation due to heat transfer and can be represented as:

$$Be = \frac{N_H}{N_G} = \frac{(\sigma_1 - 2\sigma_2 + Q_0\sigma_2)\left(\theta'(\Lambda)\right)^2}{A} \tag{37}$$

where $A = Br\left(\frac{1}{Re}\left(4C_1(F(\Lambda))^2 + 8(F(\Lambda))^2 + 2C_1\left(H'(\Lambda)\right)^2 + 4\left(H'(\Lambda)\right)^2\right) + 2\left(C_1 M(\Lambda) F'(\Lambda) + \left(F'(\Lambda)\right)^2 + \left(G'(\Lambda)\right)^2\right)\right) + (\sigma_1 - 2\sigma_2 + Q_0\sigma_2)\left(\theta'(\Lambda)\right)^2$

4 Numerical Method

The highly nonlinear ODEs governing the flow and heat transfer are difficult to solve analytically in the presence of slip conditions. In order to seek solutions for the governing equations of fluid over a rotating disk with anisotropic slip, a numerical method (bvp4c) is employed in which a MATLAB package offered by Kierzenka and Shampine [23] is used. This method has been effectively used to solve the nonlinear ODEs of various boundary value problems.

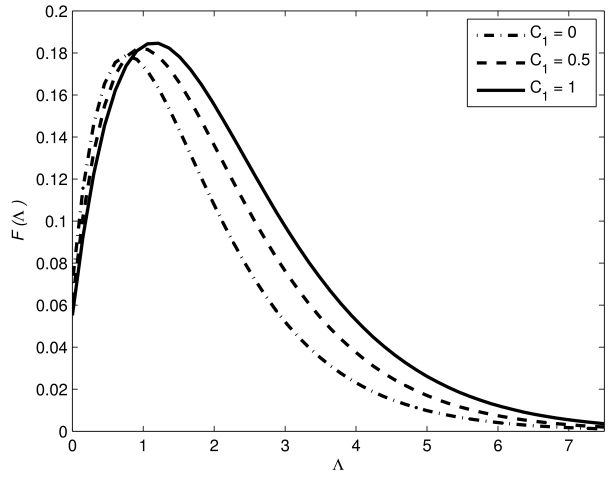

Figure 2: Effect of C_1 on $F(\Lambda)$ keeping $\zeta = \eta = 0.2$, $C_2 = C_3 = 1$, Pr = 6.8, $Br = 1$ and $Re = 2950$

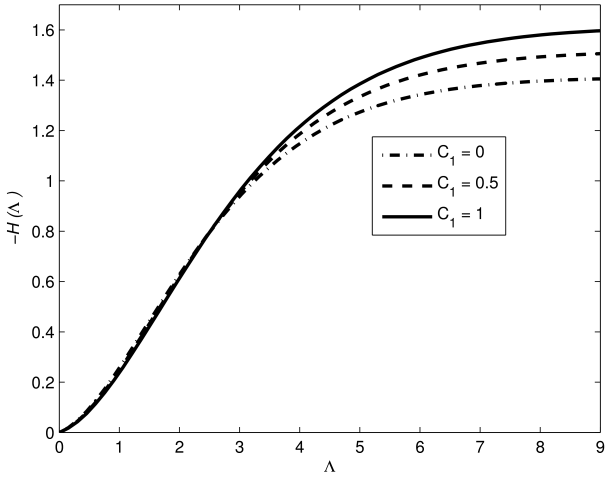

Figure 4: Effect of C_1 on $-H(\Lambda)$ keeping $\zeta = \eta = 0.2$, $C_2 = C_3 = 1$, Pr = 6.8, $Br = 1$ and $Re = 2950$

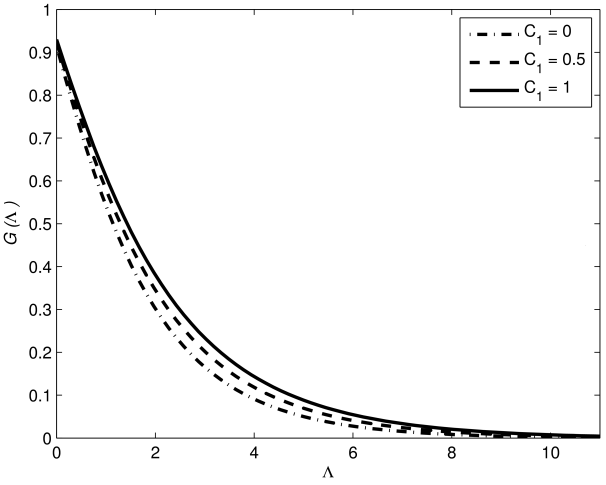

Figure 3: Effect of C_1 on $G(\Lambda)$ keeping $\zeta = \eta = 0.2$, $C_2 = C_3 = 1$, Pr = 6.8, $Br = 1$ and $Re = 2950$

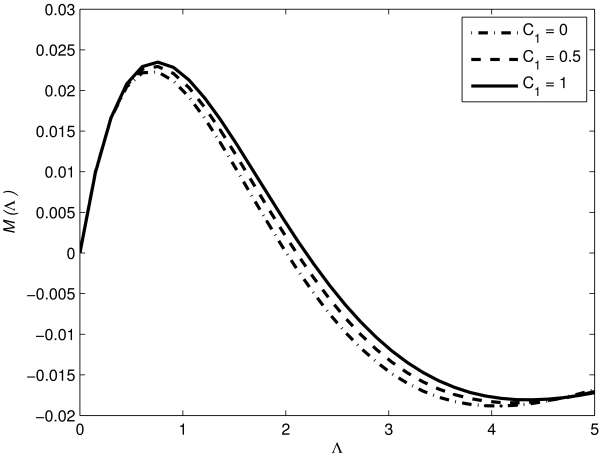

Figure 5: Effect of C_1 on $M(\Lambda)$ keeping $\zeta = \eta = 0.2$, $C_2 = C_3 = 1$, Pr = 6.8, $Br = 1$ and $Re = 2950$

5 Numerical Results and Discussion

It is highly unlikely to find an analytical solution of the coupled nonlinear equations; therefore, a numerical solutions for the velocity, microrotation, and temperature along with the anisotropic slip have been obtained using the numerical method discussed in previous section with the purpose of giving the detailed behavior of flow fields and thermal distribution. In this section, the influence of main controlling parameters present in the governing equations is discussed and the graphical representations of entropy generation and Bejan numbers have been presented to observe the effect of pertinent parameters. The considered mathematical problem defined in Eqs. (21)-(26) with the boundary conditions in Eqs. (27)-(28) have been solved by a numerical method (bvp4c) for a suitable range of the values of fluid parameters like the vortex viscosity parameter C_1, spin gradient viscosity parameter C_2, microinertia density parameter C_3, Reynolds number Re, Prandtl number Pr, Brinkman number Br, radial slip ζ and tangential slip η. The effects of theses parameters on velocity, microrotation, and temperature fields have been presented graphically through Figures 2-11. All the calculations are taken at high Reynolds number, *i.e.* $Re = 2950$.

In Figures 2-7, the effect of the vortex viscosity parameter C_1 on the velocity profiles, microrotation, and temperature distribution have been considered for $\zeta = \eta = 0.2$, $C_2 = 1$, $C_3 = 1$, Pr = 6.8, $Br = 1$ and $Re = 2950$. Figure 2 illustrates the influence of C_1 on the radial velocity $F(\Lambda)$. The radial velocity field $F(\Lambda)$ increases near the disk, then

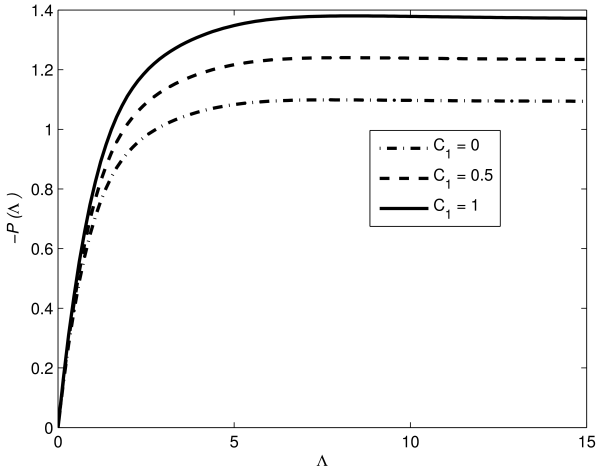

Figure 6: Effect of C_1 on $-P(\Lambda)$ keeping $\zeta = \eta = 0.2$, $C_2 = C_3 = 1$, Pr = 6.8, $Br = 1$ and $Re = 2950$

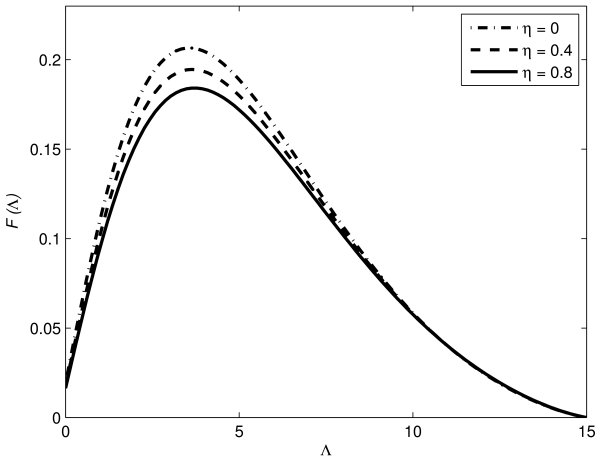

Figure 8: Effect of η on $F(\Lambda)$ keeping $\zeta = 0.2$, $C_1 = C_2 = C_3 = 20$, Pr = 6.8, $Br = 1$ and $Re = 2950$

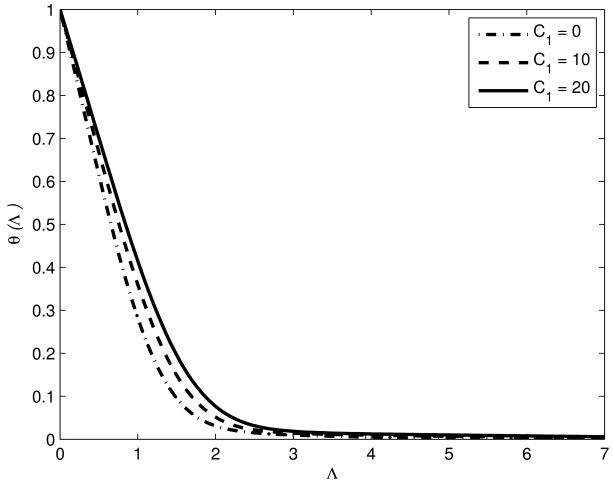

Figure 7: Effect of C_1 on $\theta(\Lambda)$ keeping $\zeta = \eta = 0.2$, $C_2 = C_3 = 1$, Pr = 6.8, $Br = 1$ and $Re = 2950$

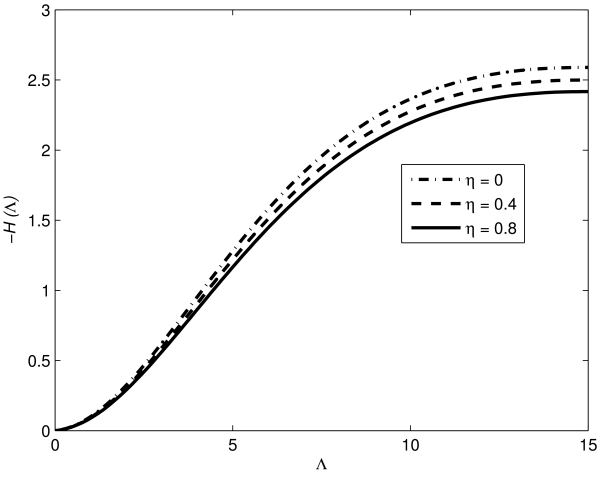

Figure 9: Effect of η on $-H(\Lambda)$ keeping $\zeta = 0.2$, $C_1 = C_2 = C_3 = 20$, Pr = 6.8, $Br = 1$ and $Re = 2950$

starts to decrease as fluid moves far from the disk and reduces to zero. Figure 3 indicates that the tangential velocity field $G(\Lambda)$ exhibits exponentially decaying behavior as the values of C_1 rise. Figure 4 shows the influence of C_1 on axial velocity $-H(\Lambda)$, which illustrates that the axial velocity $-H(\Lambda)$ increases when it moves away from the disk by increasing the values of C_1. From Figure 5, it is observed that the magnitude of microrotation, $M(\Lambda)$, increases with C_1 and these profiles decrease near the boundary and increase far from the boundary. The pressure profiles in von Kármán flows rises near the disk and become constant as they move away from the disk. The pressure profiles increase with an increase in the values of C_1 as depicted in Figure 6. The temperature profiles exhibit the increasing behavior with the higher values of C_1 as displayed in Figure 7.

The tangential velocity, microrotation profiles, pressure, and temperature distributions are not greatly affected by the slip parameters which lead us to the decision to consider the effect of these parameters on radial and axial velocity profiles only, as showed in Figures 8-9.

Figure 8 depicts the influence of tangential slip parameter η on radial velocity $F(\Lambda)$ in the presence of radial slip $\zeta = 0.2$ at $C_1 = C_2 = C_3 = 20$, Pr = 6.8, $Br = 1$, and $Re = 2950$. It is mentioned formerly that different slip lengths in span and stream-wise directions have opposite effect on fluid velocity. From Figures 8-9, it can be observed that radial and axial velocities decrease in both directions as increasing the values of tangential slip parameter η.

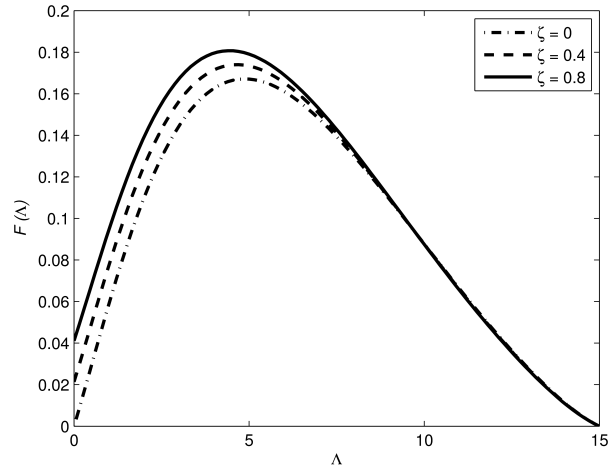

Figure 10: Effect of ζ on $F(\Lambda)$ keeping $\eta = 0.2$, $C_1 = C_2 = C_3 = 50$, Pr = 6.8, $Br = 1$ and $Re = 2950$

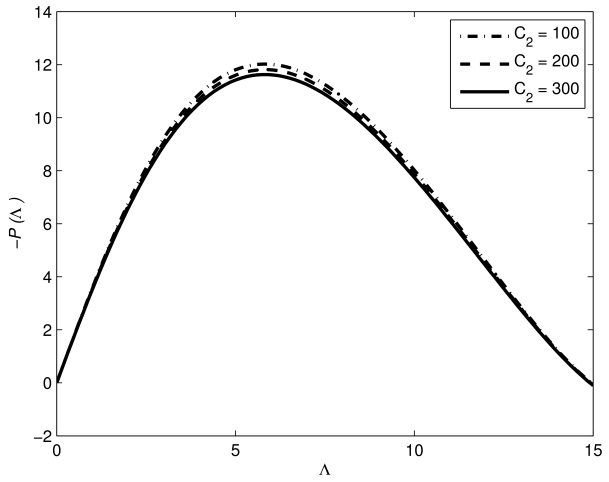

Figure 12: Effect of C_2 on $-P(\Lambda)$ keeping $\zeta = \eta = 0.2$, $C_1 = C_3 = 200$, $Br = 1$, Pr = 6.8 and $Re = 2950$

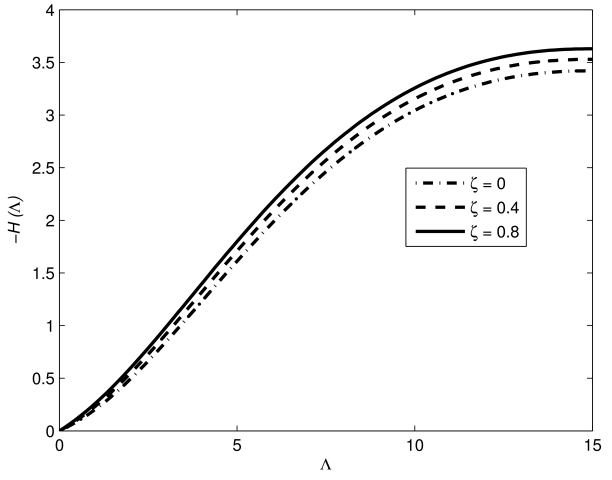

Figure 11: Effect of ζ on $-H(\Lambda)$ keeping $\eta = 0.2$, $C_1 = C_2 = C_3 = 50$, Pr = 6.8, $Br = 1$ and $Re = 2950$

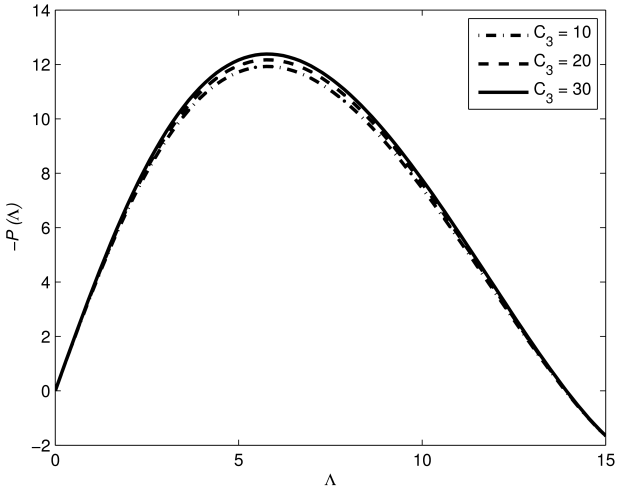

Figure 13: Effect of C_3 on $-P(\Lambda)$ keeping $\zeta = \eta = 0.5$, $C_1 = C_2 = 400$, $Br = 1$, Pr = 6.8, and $Re = 100$

In order to analyze the effects of radial slip parameter ζ on radial velocity $F(\Lambda)$ and axial velocity $-H(\Lambda)$ profiles, graphs are plotted in Figures 10-11 in the presence of tangential slip $\eta = 0.2$ and at $C_1 = C_2 = C_3 = 50$, Pr = 6.8, $Br = 1$ and $Re = 2950$. It is clearly seen that both, the radial and axial velocities increase with an increase in the values of radial slip. The reason behind this phenomenon is that the slip at the disk surface increases as the radial slip parameter ζ increases.

Figures 12-13 depict the effect of the spin gradient viscosity parameter C_2 for $C_1 = C_3 = 200$, and the influence of the microinertia density parameter C_3 for $C_1 = C_2 = 400$, keeping $Br = 1$, Pr = 6.8, and $Re = 2950$. The influences of these micropolar parameters C_2 and C_3 are observed on the pressure distribution $-P(\Lambda)$ in the presence of radial and tangential slips as $\zeta = \eta = 0.2$. The spin gradient viscosity parameter C_2 has an inverse effect on pressure distribution $-P(\Lambda)$ as shown in Figure 12, because pressure decreases by increasing the values of C_2, whereas pressure increases as raising the values of microinertia density parameter C_3.

The effect of Reynolds number Re on radial velocity $F(\Lambda)$ profiles and axial velocity $-H(\Lambda)$ profiles are exhibited through the graphs shown in Figures 14-15. The graphs are plotted in the presence of radial slip $\zeta = 0.5$, tangential slip $\eta = 0.2$ and at $C_1 = C_2 = C_3 = 50$, Pr = 6.8, $Br = 5$. It is observed that radial velocity $F(\Lambda)$ and axial velocity $-H(\Lambda)$ reduce when the Reynolds number Re changes from low to high values as displayed in Figures 14-

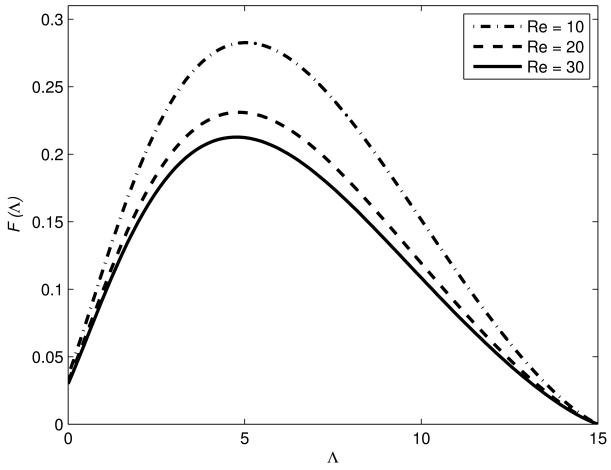

Figure 14: Effect of Re on $F(\Lambda)$ keeping $\zeta = 0.5$, $\eta = 0.2$, $C_1 = C_2 = C_3 = 50$, Pr = 6.8, and $Br = 5$

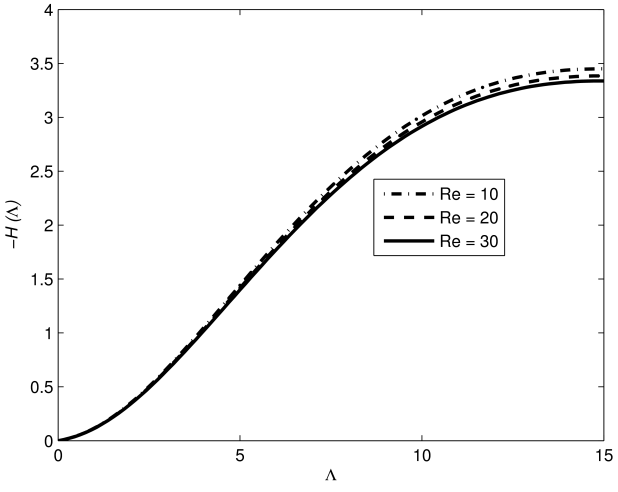

Figure 15: Effect of Re on $-H(\Lambda)$ keeping $\zeta = 0.5$, $\eta = 0.2$, $C_1 = C_2 = C_3 = 50$, Pr = 6.8, and $Br = 5$

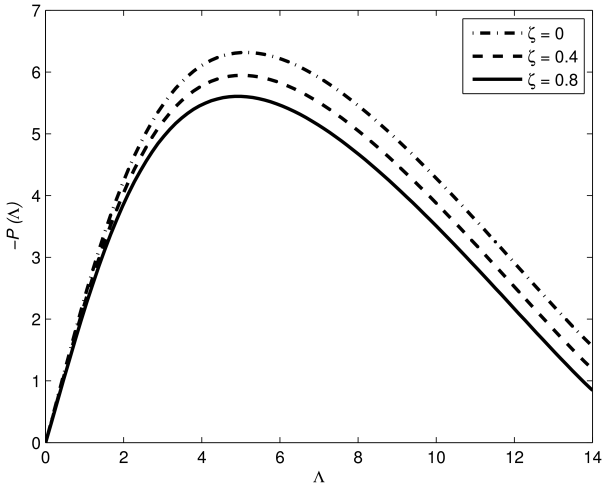

Figure 16: Effect of ζ on $-P(\Lambda)$ keeping $\eta = 0.2$, Pr = 6.8, $Br = 1$, $Re = 2950$, $C_1 = C_2 = C_3 = 50$

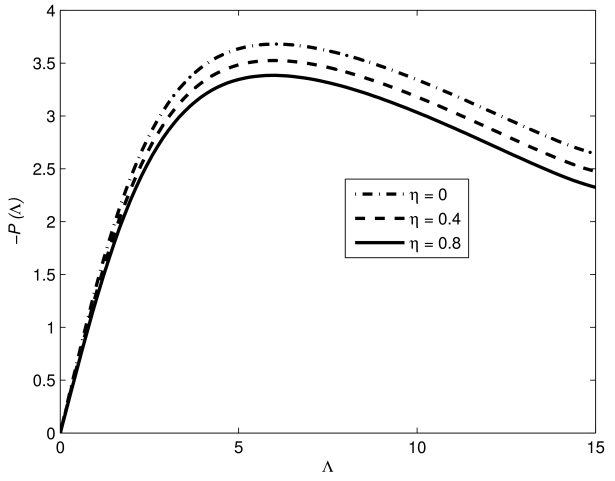

Figure 17: Effect of η on $-P(\Lambda)$ keeping $\zeta = 0.2$, Pr = 6.8, $Br = 1$, $Re = 2950$, $C_1 = C_2 = C_3 = 20$

15. Therefore, the parameter Re shows the decreasing effect on both the radial and axial velocities.

Figures 16-17 show the pressure distribution $-P(\Lambda)$ for selected values of the radial slip ζ and tangential slip η parameters.

The influence of the radial slip parameter ζ on the pressure distribution $-P(\Lambda)$ is displayed in Figure 16, which shows that an increase in the values of radial slip ζ results in the fall of pressure. It can be observed from Figure 17, that increasing the values of the tangential slip parameter η also decrease the pressure. From Figures 18-19, it is quite evident that there is an increase in temperature $\theta(\Lambda)$ with increasing the values of the Brinkman number Br as well as the microinertia density parameter C_3 in the presence of radial and tangential slips, taking $\zeta = 0.5$ and $\eta = 0.2$.

To examine the effects of Prandtl number Pr and Reynolds number Re on temperature fields $\theta(\Lambda)$, the graphs are plotted as shown in Figures 20 and 21 from which, it can be seen that the temperature profiles decrease for an increase in the values of Pr and Re.

Figure 22 gives the influence of the vortex viscosity parameter C_1 on the boundary layer thickness and it is inferred that it increases with increasing the values of vortex viscosity parameter. The circumferential velocity is employed to observe the boundary layer thickness for von Kármán flows of Newtonian fluids, which occurs at the point where the tangential velocity drops to $G \approx 0.01$ as referred in [24].

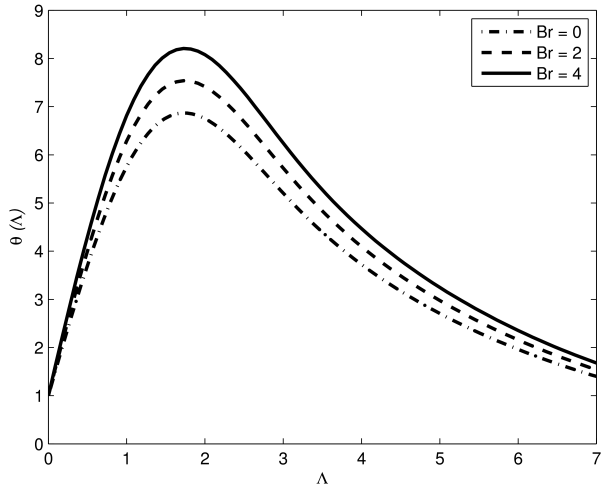

Figure 18: Effect of Br on $\theta(\Lambda)$ keeping $\zeta = 0.5$, $\eta = 0.2$, $C_1 = C_2 = C_3 = 100$, Pr = 6.8, $Re = 100$

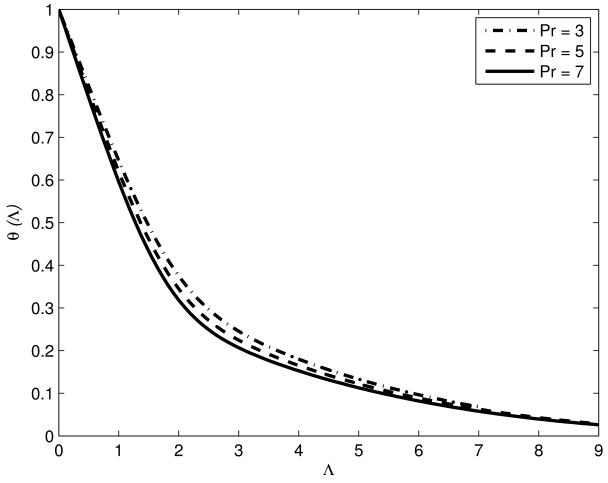

Figure 20: Effect of Pr on $\theta(\Lambda)$ keeping $\zeta = 0.5$, $\eta = 0.2$, $C_1 = C_2 = C_3 = 400$, $Br = 1$, $Re = 40$

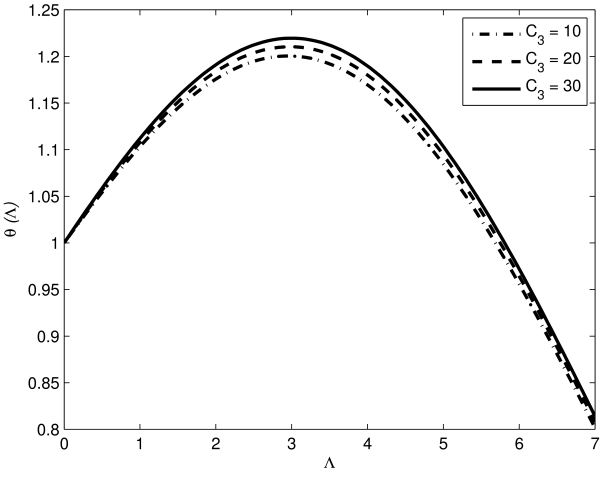

Figure 19: Effect of C_3 on $\theta(\Lambda)$ keeping $\zeta = 0.5$, $\eta = 0.2$, $C_1 = C_2 = 400$, Pr = 6.8, $Br = 1$, $Re = 100$

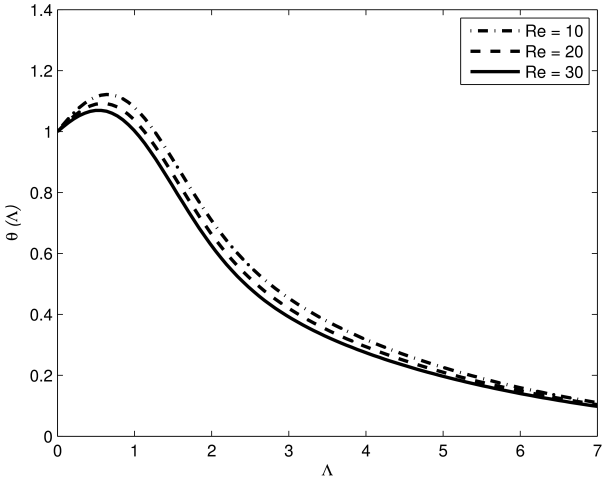

Figure 21: Effect of Re on $\theta(\Lambda)$ keeping $\zeta = 0.5$, $\eta = 0.2$, $C_1 = C_2 = C_3 = 50$, $Br = 5$, Pr = 6.8

Figures 23-28 exhibit the pronounced variation of entropy generation number N_G and the Bejan number Be associated with the effects of Brinkman number Br, vortex viscosity parameter C_1, and Prandtl number Pr. Figure 23 demonstrates the variation of the entropy generation number, which varies with the increasing values of Brinkman number, which gives its maximum value near the disk and decreases away from the disk. The opposite behavior is shown in Figure 24. The Bejan number decreases as the Brinkman increases.

It is illustrated by Figures 25-26 that the entropy generation and the Bejan numbers decrease near the disk as C_1 increases. The influence of the Prandtl number on the entropy generation number and the Bejan number are presented in Figure 27-28. The entropy generation number increases with Prandtl number as depicted in Figure 27. A rise in the values of Prandtl number increases the Bejan number but it becomes minimum as fluid moves away from the disk as shown in Figure 28.

Table 1 presents numerical values for local skin friction coefficients C_f and C_g, and local Nusselt number N_u for different pertinent parameters. The vortex viscosity parameter C_1 decreases both the skin friction coefficients and Nusselt number, which increases the fluid flow over disk and heat transfer increases as a decrement in the Nusselt number. The increase in the values of spin gradient viscosity parameter C_2 increases the skin friction coefficient C_f, which reduces the fluid flow in the radial direction and also increases the Nusselt number, while skin friction coefficient C_g diminishes allowing more fluid to flow

Table 1: Numerical values of local skin friction coefficients C_f and C_g, local Nusselt number N_u for physical parameters C_1, C_2, C_3, ζ, η and Pr while keeping $Re = 2950$ and $Br = 1$

C_1	C_2	C_3	ζ	η	Pr	$Re^{-\frac{1}{2}}C_f$	$Re^{-\frac{1}{2}}C_g$	$Re^{-\frac{1}{2}}N_u$
0	10	10	0.2	0.2	6.2	0.3526	0.5837	0.6413
10						0.1291	0.1898	0.6642
20						0.0925	0.1401	0.5891
10	10	10	0.2	0.2	6.2	0.1291	0.1898	0.6642
	20					0.1316	0.1883	0.6757
	30					0.1329	0.1876	0.6815
10	10	0	0.2	0.2	6.2	0.1360	0.1838	0.6985
		10				0.1291	0.1898	0.6642
		20				0.1265	0.1915	0.6510
10	10	10	0.0	0.2	6.2	0.1356	0.1825	0.5639
			0.2			0.1291	0.1898	0.6642
			0.4			0.1231	0.1963	0.7506
10	10	10	0.2	0.0	6.2	0.1369	0.2012	0.6692
				0.2		0.1291	0.1898	0.6642
				0.4		0.1223	0.1798	0.6590
10	10	10	0.2	0.2	1	0.1291	0.1898	0.1871
					3	0.1291	0.1898	0.4421
					5	0.1291	0.1898	0.5928

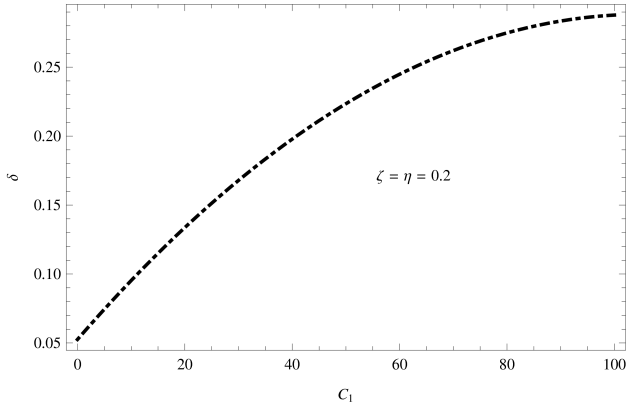

Figure 22: Effect of vortex viscosity parameter C_1 on boundary layer thickness δ keeping $\zeta = \eta = 0.2$, $C_2 = C_3 = 10$, $Br = 1$, Pr = 6.8, Re = 2950

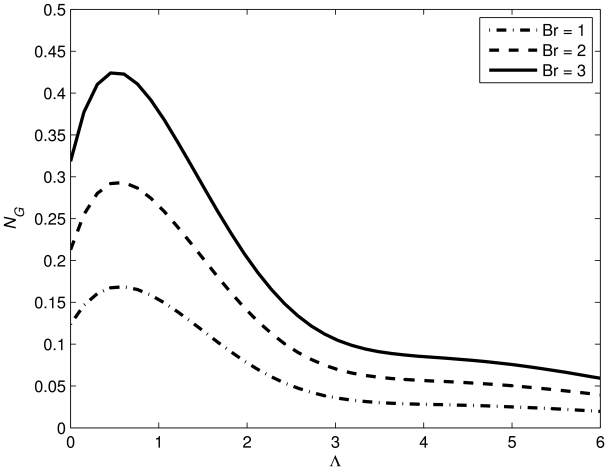

Figure 23: Effect of Br on N_G keeping $\zeta = \eta = 0.2$, $C_1 = C_2 = C_3 = 10$, $Br = 1$, Pr = 6.8, $Re = 2950$, $\sigma_1 = 1$, $\sigma_2 = 0.5$, $Q_0 = 0.5$

in a tangential direction. The radial skin friction coefficient and Nusselt number decrease as the values of the microinertia density parameter C_3 increase, whereas skin friction coefficient increases in the tangential direction. The skin friction coefficient decreases for increasing values of radial slip parameter ζ, which allows more fluid to flow in a radial direction. On the other hand, the tangential skin friction and Nusselt number increase, which reduces the flow in a tangential direction. The increasing effect in the values of tangential slip parameter η decreases both the physical quantities like skin friction coefficient and Nusselt number. Therefore, fluid velocity increases with increase in the tangential slip parameter. Finally, it is observed that variations in the Prandtl number Pr change the Nusselt number only, which reduces heat transfer as the Nusselt number increases.

For the reliability of numerical outcomes, comparison of the present results with [24] is presented in Table 2. It can be seen that the results are in good agreement at $C_1 = C_2 = C_3 = \zeta = \eta = 0$, which validates the re-

Table 2: Numerical comparison of some physical quantities with Ref. [24] obtained at $Re = 2950$

Physical Quantities	[24]	$C_1 = C_2 = C_3 = 0$ $\zeta = \eta = 0$	$C_1 = 5, C_2 = C_3 = 0$ $\zeta = \eta = 0$	$C_2 = 10C_1 = C_3 = 0$ $\zeta = \eta = 0$	$C_1 = C_2 = C_3 = 0$ $\zeta = 0.2, \eta = 0$	$C_1 = C_2 = C_3 = 0$ $\zeta = 0, \eta = 0.2$	$C_1 = C_2 = C_3 = 10$ $\zeta = 0.2, \eta = 0.2$
$F'(0)$	0.51023	0.5102	0.2081	0.5102	0.4201	0.4324	0.1291
$-G'(0)$	0.61592	0.6159	0.2511	0.6159	0.7076	0.5220	0.1898
$-H(\infty)$	0.8838	0.8844	2.0730	0.8844	0.9324	0.8370	2.4870
$-P(\infty)$	0.3906	0.3911	2.1487	0.3911	0.2667	0.3502	2.7828
$Re^{-\frac{1}{2}}\delta$	5.4	5.25	12.0	5.4	4.95	5.55	13.65

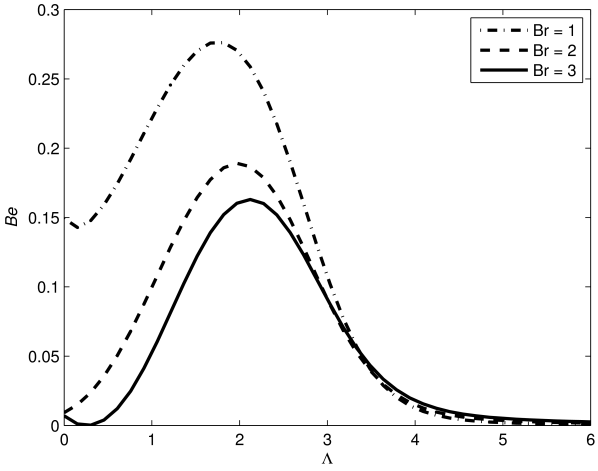

Figure 24: Effect of Br on Be keeping $\zeta = \eta = 0.2$, $C_1 = C_2 = C_3 = 10$, $Br = 1$, Pr = 6.8, $Re = 2950$, $\sigma_1 = 1$, $\sigma_2 = 0.5$, $Q_0 = 0.5$

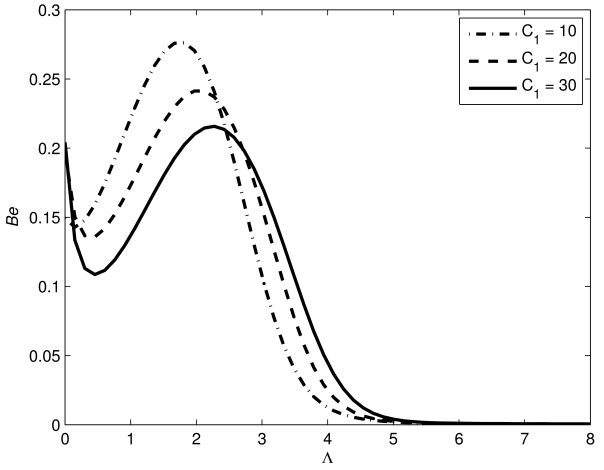

Figure 26: Effect of C_1 on Be keeping $\zeta = \eta = 0.2$, $C_2 = C_3 = 10$, $Br = 1$, Pr = 6.8, $Re = 2950$, $\sigma_1 = 1$, $\sigma_2 = 0.5$, $Q_0 = 0.5$

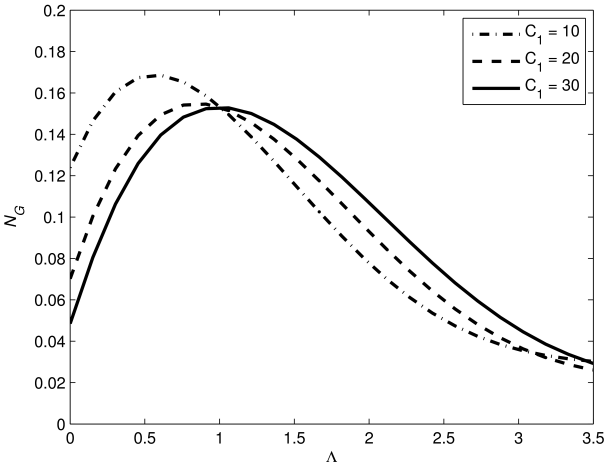

Figure 25: Effect of C_1 on N_G keeping $\zeta = \eta = 0.2$, $C_2 = C_3 = 10$, $Br = 1$, Pr = 1.5, $Re = 2950$, $\sigma_1 = 1$, $\sigma_2 = 0.5$, $Q_0 = 0.5$

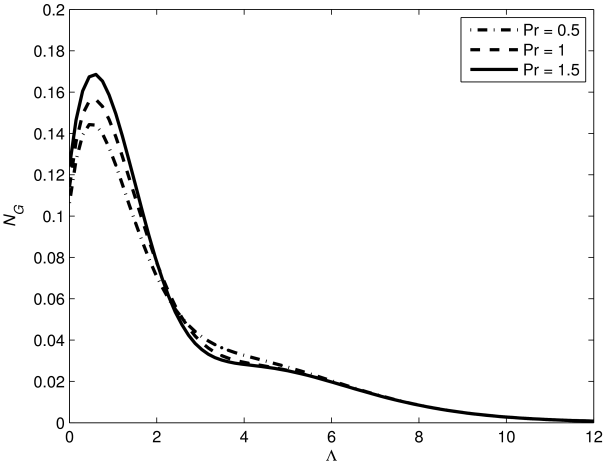

Figure 27: Effect of Pr on N_G keeping $\zeta = \eta = 0.2$, $C_1 = C_2 = C_3 = 10$, Pr = 6.8, $Re = 2950$, $\sigma_1 = 1$, $\sigma_2 = 0.5$, $Q_0 = 0.5$

sults and computational technique. This table also shows the effects of four other parameters by varying the value of one parameter while the others are kept at zero. It is observed that the vortex viscosity parameter C_1 has a decreasing effect on radial and tangential skin frictions while it increases the volumetric flow rate, pressure, and bound-

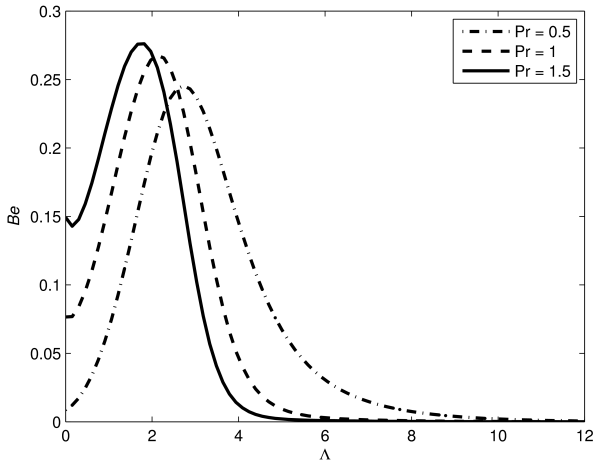

Figure 28: Effect of Pr on Be keeping $\zeta = \eta = 0.2$, $C_1 = C_2 = C_3 = 10$, $Br = 1$, $Re = 2950$, $\sigma_1 = 1$, $\sigma_2 = 0.5$, $Q_0 = 0.5$

ary layer thickness for $C_1 = 5$. On the other hand, when the spin gradient viscosity parameter is fixed at $C_2 = 10$, it gives the same results as obtained in [24] but it changes the volumetric flow rate from 0.8838 to 0.8844 and the pressure from 0.3906 to 0.3911. The radial skin friction, pressure, and boundary layer thickness are found decreasing for $\zeta = 0.2$, while it enhances the tangential skin friction and volumetric flow rate. The tangential slip parameter illustrates the decreasing behavior on all the quantities except boundary layer thickness, which slightly increases from 5.4 to 5.55 at $\eta = 0.2$. It can be seen that radial and tangential skin friction reduce for $C_1 = C_2 = C_3 = 10$, and $\zeta = \eta = 0.2$, while it increases the volumetric flow rate, pressure, and boundary layer thickness.

6 Conclusion

The present work examined the flow of an incompressible micropolar fluid over a rotating disk in the existence of anisotropic slip conditions and dissipation. The flow, microrotation, and temperature fields have been computed by considering the effects of most significant parameters including the spin gradient viscosity, vortex viscosity, microinertia density, Reynolds number, Brinkman number, Prandtl number, and radial and tangential slips. The details of the flow, microrotation, and heat transfer characteristics have been illustrated by numerical results. The following results have been concluded from the investigation of the considered problem:

(i) The radial, tangential, and, axial velocities increased for the rising values of vortex viscosity parameter C_1. The microrotation, temperature, and pressure also increased with an increase in C_1.

(ii) The radial and axial velocities and pressure decreased with the increase in the tangential slip parameter η.

(iii) The increasing values of the radial slip parameter ζ have increased the radial and axial velocities but have decreased the pressure.

(iv) The pressure and temperature increased by increasing the values of the microinertia density parameter C_3 but pressure showed inverse effect when the values of the spin gradient viscosity parameter C_2. were increased.

(v) The radial and axial velocities as well as the temperature decreased by increasing the Reynolds number Re.

(vi) The temperature increased on increasing the values of Brinkman number Br but decreased when the values of Prandtl number Pr were increased.

(vii) The boundary layer thickness increased by increasing the values of the vortex viscosity parameter C_1.

(viii) The Entropy generation and Bejan numbers were also obtained and illustrated explicitly for different values of pertinent parameters.

(ix) A favorable agreement has been observed when comparing the numerical results of the present study with previously published studies.

References

[1] Eringen, AC, Simple microfluids, International Journal of Engineering Science, 2 (1964) 205-217.

[2] Eringen, AC, Theory of micropolar fluids, DTIC Document, 1965.

[3] Eringen, AC, Theory of thermomicrofluids, Journal of Mathematical Analysis and Applications, 38 (1972) 480-496.

[4] Lukaszewicz, G, Micropolar fluids: theory and applications, Springer Science & Business Media, 1999.

[5] Stokes, VK, Micropolar Fluids, in: Theories of Fluids with Microstructure: An Introduction, Springer Berlin Heidelberg, Berlin, Heidelberg, (1984) 150-178.

[6] Ariman, T, Turk, MA, Sylvester, ND, Microcontinuum fluid mechanics-a review, International Journal of Engineering Science, 11 (1973) 905-930.

[7] Chamkha, AJ, Jaradat, M, Pop, I, Three-dimensional micropolar flow due to a stretching flat surface, International Journal of Fluid Mechanics Research, 30 (2003) 357-366.

[8] Ashraf, M, Batool, K, MHD flow and heat transfer of a micropolar fluid over a stretchable disk, Journal of theoretical and applied mechanics, 51 (2013) 25-38

[9] Borrelli, A, Giantesio, G, Patria, MC, Numerical simulations of three-dimensional MHD stagnation-point flow of a micropolar fluid, Computers & Mathematics with Applications, 66 (2013) 472-489.

[10] Hussain, S, Kamal, MA, Ahmad, F, The accelerated rotating disk in a micropolar fluid flow, Applied Mathematics, 05 (2014) 196-202.
[11] Kármán, TV, Über laminare und turbulente Reibung, ZAMM-Journal of Applied Mathematics and Mechanics, 1 (1921) 233-252.
[12] Turkyilmazoglu, M, MHD fluid flow and heat transfer due to a stretching rotating disk, International Journal of Thermal Sciences, 51 (2012) 195-201.
[13] Ming, C, Zheng, L, Zhang, X, Steady flow and heat transfer of the power-law fluid over a rotating disk, International Communications in Heat and Mass Transfer, 38 (2011) 280-284.
[14] Rashidi, MM, Hayat, T, Erfani, E, Mohimanian Pour, SA, Hendi, AA, Simultaneous effects of partial slip and thermal-diffusion and diffusion-thermo on steady MHD convective flow due to a rotating disk, Communications in Nonlinear Science and Numerical Simulation, 16 (2011) 4303-4317.
[15] Bejan, A, A study of entropy generation in fundamental convective heat transfer, Journal of Heat Transfer, 101 (1979) 718-725.
[16] Bejan, A, Entropy generation minimization: the method of thermodynamic optimization of finite-time systems and finite-time processes, New York: CRC Press, 51 (1996) 169-180.
[17] Abdollahzadeh Jamalabadi, MY, Entropy generation in boundary layer flow of a micro polar fluid over a stretching sheet embedded in a highly absorbing medium, Frontiers in Heat and Mass Transfer, 6 (2015).
[18] Joseph, DD, Boundary conditions for thin lubrication layers, Physics of Fluids, 23 (1980) 2356-2358.
[19] Das, K, Acharya, N, Kundu, PK, MHD micropolar fluid flow over a moving plate under slip conditions: An application of Lie group analysis, UPB Scientific Bulletin, Series A: Applied Mathematics and Physics 78 (2016) 225-234.
[20] Bhattacharyya, K, Mukhopadhyay, S, Layek, GC, Slip effects on boundary layer stagnation-point flow and heat transfer towards a shrinking sheet, International Journal of Heat and Mass Transfer, 54 (2011) 308-313.
[21] Wang, CY, Ng, C-O, Slip flow due to a stretching cylinder, International Journal of Non-Linear Mechanics, 46 (2011) 1191-1194.
[22] Busse, A, Sandham, ND, Influence of an anisotropic slip-length boundary condition on turbulent channel flow, Physics of Fluids, 24 (2012) 055111.
[23] Kierzenka, J, Shampine, LF, A BVP solver based on residual control and the Maltab PSE, ACM Transactions on Mathematical Software 27 (2001) 299-316.
[24] White, FM, Viscous fluid flow, Second ed., McGraw-Hill, Incorporated, Singapore, 1991.